

Estimation of dynamic fatigue strengths in brittle materials under a wide range of stress rates

Shinya Matsuda · Ryosuke Watanabe

Received: 12 January 2011 / Accepted: 1 March 2011 / Published online: 11 March 2011
© Springer Science+Business Media, LLC 2011

Abstract This paper aims to statistically estimate the dynamic fatigue strength in brittle materials under a wide range of stress rates. First, two probabilistic models were derived on the basis of the slow crack growth (SCG) concept in conjunction with two-parameter Weibull distribution. The first model, Model I, is a conventional probabilistic delayed-fracture model based on a concept wherein the length of the critical crack growth due to SCG is enough larger than the initial crack length. For the second model, Model II, a new probabilistic model is derived on the basis of a concept wherein the critical cracks have widely ranging lengths. Next, a four-point bending test using a wide range of stress rates was performed for soda glass and alumina ceramics. We constructed fracture probability–strength–time diagrams (F–S–T diagrams) with the experimental results of both materials using both models. The F–S–T diagrams described using Model II were in good agreement with plots of the fracture strength and the fracture time of both materials more so than Model I.

Introduction

Ceramics have excellent mechanical properties, i.e. heat resistance, wear resistance, and high specific strengths. Therefore, ceramics have been widely applied as various engineering components and electronic devices. Consequently, with the

increase in the applications using ceramics, estimating the strength associated with damage and fracture has become even more essential for saving reliability.

Slow crack growth (SCG) is a well-known phenomenon in brittle materials with numerous cracks of various sizes. A widely used empirical relation models the stress intensity factor at the crack tip and the rate of SCG. The model (SCG law) covers the SCG rates that are most interesting for estimating dynamic, static, and cyclic fatigue strength in brittle materials. Therefore, many studies estimating the fatigue strength in brittle materials, such as fine ceramics and glasses, have been conducted on the basis of SCG law [1–10].

Subsequently, for statistically estimating the static fatigue strength and the cyclic fatigue strength in brittle materials, various probabilistic models have been proposed on the basis of SCG law in conjunction with Weibull distribution for considering large scatters of the fatigue strength [11–15]. However, there are very few studies that statistically estimate the dynamic fatigue strength in brittle materials under a wide range of stress rates [16].

The purpose of this study was to statistically estimate the dynamic fatigue strength in brittle materials under a wide range of stress rates. First, two probabilistic models were derived on the basis of SCG law in conjunction with a two-parameter Weibull distribution. The first model, Model I, is a conventional probabilistic delayed-fracture model based on the concept wherein the length of the critical crack growth due to SCG is enough larger than the initial crack length. The second model, Model II, is derived on the basis of the concept wherein the critical crack lengths range broadly. Next, a four-point bending test using a wide range of stress rates was performed for soda glass and alumina ceramics. We compared fracture probability–strength–time diagrams (F–S–T diagrams) for both models described with the experimental results.

S. Matsuda (✉) · R. Watanabe
Department of Mechanical Engineering, Numazu National
College of Technology, 3600 Ooka, Numazu, Shizuoka
410-8501, Japan
e-mail: matsuda@numazu-ct.ac.jp

Modeling

Here, we derived two models to statistically estimate the dynamic fatigue strength in brittle materials. In Model I, a conventional probabilistic delayed-fracture model is derived on the basis of the concept wherein the length of the critical crack growth due to SCG is enough larger than the initial crack length [15]. Model II is derived on the basis of the concept wherein the critical crack lengths range widely.

Model I

The SCG behavior of an initial crack in a brittle material under applied stress $\sigma(t)$ is formulated on the basis of the fracture mechanics model established by Evans and Fuller [17]. The stress intensity factor K_I of a crack of length a is expressed as

$$K_I = Y\sigma(t)\sqrt{a} \quad (1)$$

where Y is a constant depending on the geometry of the crack. SCG law that describes the relationship between the crack propagation rate (SCG rate) v and K_I is given by

$$v = \frac{da}{dt} = C \left(\frac{K_I}{K_{IC}} \right)^n \quad (2)$$

where K_{IC} , C , and n denote the fracture toughness, crack propagation rate at K_{IC} , and crack propagation index, respectively. When the critical crack length, a_f , growing due to SCG, is large enough, integrating Eq. 2 using Eq. 1 gives

$$C\lambda\alpha^n\sigma_{max}^n \int_0^{t_f} \left(\frac{\sigma(t)}{\sigma_{max}} \right)^n dt \approx a_i^{-\lambda} \quad (3)$$

where a_i , σ_{max} , and t_f are the initial crack length, the fracture strength, and the time until unstable crack growth, respectively. In addition, λ and α equal $(n - 2)/2$ and Y/K_{IC} , respectively. In Eq. 3, a_i is related to K_{IC} , and the real, fast (or inert) fracture strength S_i as

$$a_i = \left(\frac{K_{IC}}{YS_i} \right)^2 \quad (4)$$

Substituting Eq. 4 into Eq. 3, the real, fast fracture strength S_i^* for σ_{max} and the effective loading time, t_{eff} , leads to

$$S_i^* = (C\lambda\alpha^2\sigma_{max}^n t_{eff})^{1/2\lambda} \quad (5)$$

where t_{eff} denotes

$$t_{eff} = \int_0^{t_f} \left(\frac{\sigma(t)}{\sigma_{max}} \right)^n dt \quad (6)$$

Next, we considered a brittle material with numerous cracks as initial defects. When S_i of the material obeys a

two-parameter Weibull distribution, the fracture probability, F , of the material is expressed as

$$F = 1 - \exp \left[- \left(\frac{S_i}{S_o} \right)^m \right] \quad (7)$$

where m and S_o denote the shape and scale parameters, respectively. Replacing S_i in Eq. 7 with S_i^* from Eq. 5 gives the fracture probability at σ_{max} and t_{eff} as

$$F = 1 - \exp \left[- \left(\frac{(C\lambda\alpha^2\sigma_{max}^n t_{eff})^{1/2\lambda}}{S_o} \right)^m \right] \quad (8)$$

Here, S_o is related to the fracture toughness K_{IC}^* and the mode value a_o of a_i in the material as

$$K_{IC}^* = Y S_o \sqrt{a_o} \quad (9)$$

Replacing K_{IC} with the material constant α of Eq. 8 and K_{IC}^* of Eq. 9, we obtain the following two-parameter Weibull distribution:

$$F = 1 - \exp \left[- \left(\frac{\sigma_{max} t_{eff}^{1/n}}{\hat{\sigma}_o} \right)^{\hat{m}} \right] \quad (10)$$

with

$$\hat{\sigma}_o = S_o t_o^{1/n}, \quad \hat{m} = mn/2\lambda, \quad t_o = 1/C\lambda a_o^{-1} \quad (11)$$

where \hat{m} and $\hat{\sigma}_o$ are Weibull parameters and t_o is the time parameter of the material, and

$$\tilde{\sigma}_f = \sigma_{max} t_{eff}^{1/n} \quad (12)$$

agrees with the normalized strength proposed by Okabe et al. [14, 15]. Using Eq. 12, cyclic, static, and dynamic fatigue strength can be converted into the fracture strength for 1 s. Finally, the normalized strength to fracture probability in Eq. 10 can be expressed as

$$\sigma_{max} t_{eff}^{1/n} = \hat{\sigma}_o \sqrt[n]{-\ln(1 - F)} \quad (13)$$

Here, Okabe proposed that though $\hat{m} = mn/2\lambda$ in Eq. 13 is almost equal to the value of m because n is large in ceramics, the normalized strength to fracture probability can be expressed from Eq. 13 as

$$\sigma_{max} t_{eff}^{1/n} = \hat{\sigma}_o \sqrt[m]{-\ln(1 - F)} \quad (14)$$

This estimation method using Eq. 14 is called the unified strength estimation method.

Model II

In Model II, we consider that the critical crack lengths growing because of SCG have a wide range. Then directly integrating Eq. 2 using Eq. 1 obtains

$$C\lambda\alpha^n\sigma_{\max}^n t_{\text{eff}} = a_i^{-\lambda} - a_f^{-\lambda} \quad (15)$$

where a_f is the critical crack length. The critical crack length is related to fracture toughness K_{IC} and the fracture strength σ_{\max} as

$$a_f = \left(\frac{K_{\text{IC}}}{Y\sigma_{\max}} \right)^2 \quad (16)$$

Substituting Eq. 4 and 16 into Eq. 15 and replacing K_{IC} of the material constant, α , in Eq. 15 with K_{IC}^* in Eq. 9, the real, fast fracture strength S_i^{**} for the fracture strength, σ_{\max} , and the effective loading time, t_{eff} , leads to

$$S_i^{**} = \sigma_{\max} \left(1 + \left[\frac{\sigma_{\max}}{S_o} \right]^2 \frac{t_{\text{eff}}}{t_o} \right)^{1/2\lambda} \quad (17)$$

Replacing S_i in Eq. 7 with S_i^{**} from Eq. 17 gives the fracture probability at σ_{\max} and t_{eff} as

$$F = 1 - \exp \left[- \left(\frac{\sigma_{\max} \left(1 + [\sigma_{\max}/S_o]^2 (t_{\text{eff}}/t_o) \right)^{1/2\lambda}}{S_o} \right)^m \right] \quad (18)$$

Rewriting Eq. 18 in the same form as the two-parameter Weibull distribution in Eq. 10 reduces to

$$F = 1 - \exp \left[- \left(\frac{\sigma_{\max} t_{\text{eff}}^{1/n} \left(1 + [S_o/\sigma_{\max}]^2 (t_o/t_{\text{eff}}) \right)^{1/n}}{\hat{\sigma}_o} \right)^{\hat{m}} \right] \quad (19)$$

where

$$\tilde{\sigma}_f^* = \sigma_{\max} t_{\text{eff}}^{1/n} \left(1 + \left[\frac{S_o}{\sigma_{\max}} \right]^2 \frac{t_o}{t_{\text{eff}}} \right)^{1/n} \quad (20)$$

agrees with the fracture strength for 1 s. We called Eq. 20 the equivalent fracture strength. The equivalent fracture strength denotes that cyclic, static, and dynamic fatigue strength are converted into the fracture strength for 1 s as well as the normalized strength. Finally, the equivalent fracture strength of the fracture probability can be expressed as

$$\sigma_{\max} t_{\text{eff}}^{1/n} \left(1 + \left[\frac{S_o}{\sigma_{\max}} \right]^2 \frac{t_o}{t_{\text{eff}}} \right)^{1/n} = \hat{\sigma}_o \sqrt[\hat{m}]{- \ln(1 - F)} \quad (21)$$

Experimental procedures

Specimens

Commercially available soda glass and alumina ceramics were used. We cut the soda glass to a size of

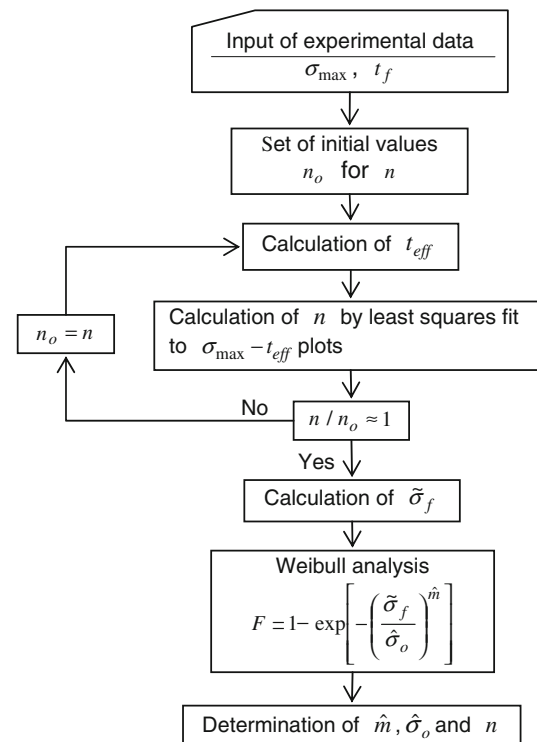


Fig. 1 Flowchart to determine the material constants with Model I

"6 × "5 × "40 mm using a diamond cutter. Here, we did not chamfer the corners of the soda glass specimen. Thereafter, the soda glass specimen was adequately dried at room temperature. On the other hand, the alumina ceramics was cut to a size of "4 × "3 × "40 mm based on the JIS6102 via a processing request.

Test method

The four-point bending test was performed for both specimens using a wide range of crosshead speeds from 1000 mm/min to 0.001 mm/min at room temperature. A wide range of stress rates $\dot{\sigma}$ was estimated at ratio of the four-point bending fracture strength σ_{\max} to the fracture time t_f . The σ_{\max} was calculated as

$$\sigma_{\max} = \frac{3P_f(L_1 - L_2)}{2wt^2} \quad (22)$$

where P_f , L_1 , and L_2 denote the fracture load, the under span of 30 mm, and the upper span of 10 mm, respectively.

Determination methods of material constants in both models

Material constants in Model I

Figure 1 depicts a flowchart for determining the material constants in Model I. The material constants were determined

using the experimental data of both materials as follows. When the fracture probability F in Eq. 10 nearly equaled 63.2%, the relationship between the fracture strength σ_{\max} and the effective loading time, t_{eff} , is simply given as

$$\frac{t_{\text{eff}}}{t_0} = \left(\frac{\sigma_{\max}}{S_0} \right)^{-n} \quad (23)$$

where t_{eff} under a constant stress rate is given as

$$t_{\text{eff}} = \frac{t_f}{n+1} \quad (24)$$

First, the crack propagation index, n , provides that the slope of the least squares fit to the plots of the fracture strength, σ_{\max} , and the effective loading time, t_{eff} , in the experimental data on a double logarithmic chart was repeatedly calculated. Next, the shape and scale parameters \hat{m} and $\hat{\sigma}_o$ in Eq. 10 were determined from a Weibull analysis of the normalized strength $\tilde{\sigma}_f$ and then converted into the fracture strength for 1 s using the fracture strength and calculated effective loading time in the experimental data and calculated n .

Material constants in Model II

Figure 2 depicts a flowchart for determining the material constants in Model II. The material constants

were determined using the experimental data of both materials as follows. Assuming that $t_{\text{eff}} \approx 0$ in Eq. 18 reduced to

$$F = 1 - \exp \left[- \left(\frac{\sigma_{\max}}{S_0} \right)^m \right] \quad (25)$$

the scale parameter, S_0 , is determined by the Weibull analysis of the fracture strength, σ_{\max} , that is obtained in the four-point bending test under very fast stress rates. Next, when $F = 63.2\%$, Eq. 18 is rewritten as

$$y = \ln\left(\frac{S_0}{\sigma_{\max}}\right) = \frac{1}{n-2} \ln\left(1 + t_o^{-1} \sigma_{\max}^2 t_{\text{eff}}\right) \quad (26)$$

First, ratios of the calculated S_o to the fracture strength, σ_{\max} , on the left-hand side of Eq. 26 are plotted against $x = \sigma_{\max}^2 t_{\text{eff}}$ for the value of the crack propagation index n . Second, curve fitting of these plots in the form of the equation $y = \{\ln(1 + x/t_0)\}/(n - 2)$ is performed. The material parameters of n and t_0 are provided by repeating these plots and curve fittings. Finally, the shape and scale parameters, \hat{m} and $\hat{\sigma}_o$, in Eq. 19 are determined from the Weibull analysis of the equivalent fracture strength $\tilde{\sigma}_f^*$ that is converted into the fracture strength for 1 s using the fracture strength, the effective loading time, and the calculated material constants of n , t_0 , and S_o .

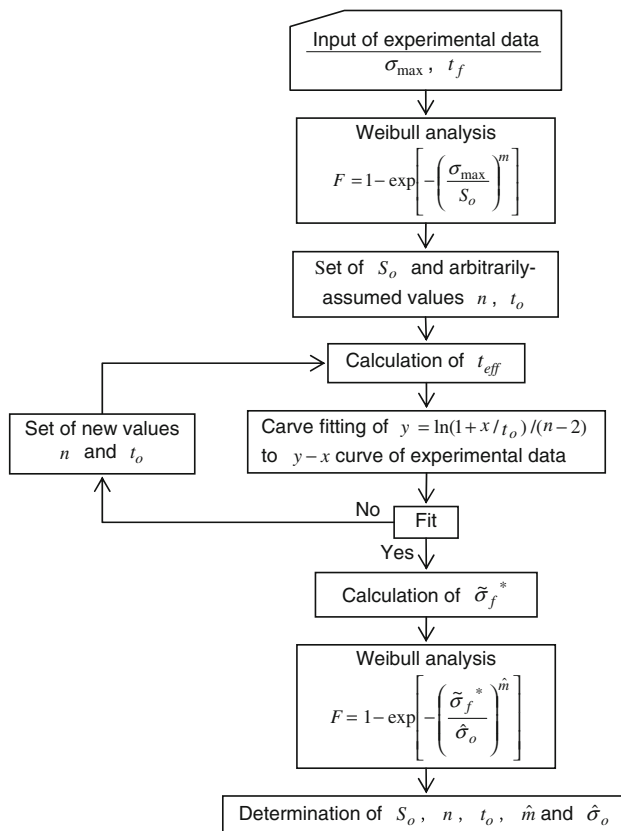


Fig. 2 Flowchart to determine the material constants with Model II

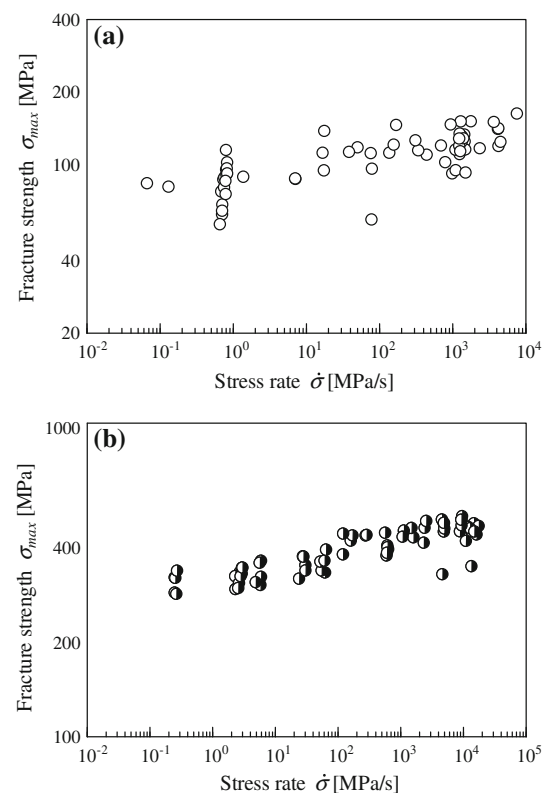


Fig. 3 σ_{\max} - $\dot{\sigma}$ plots of **a** soda glass and **b** alumina ceramics

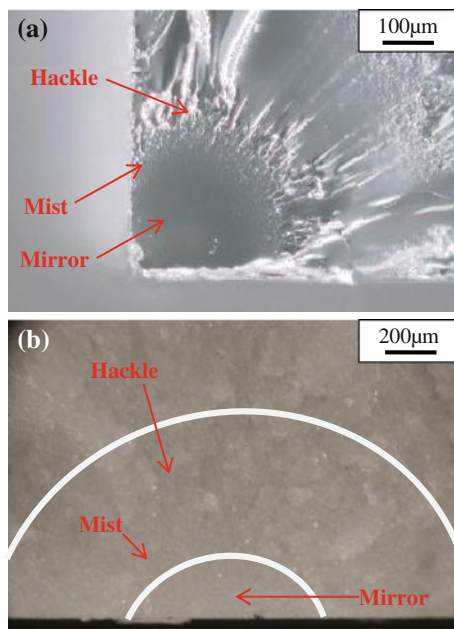


Fig. 4 Stereomicroscope images of the fracture surface of **a** soda glass and **b** alumina ceramics

Results and discussion

Dynamic fatigue behavior

Figure 3 shows the relationships between the fracture strength, σ_{\max} , and the stress rate, $\dot{\sigma}$, for soda glass and alumina ceramics. The fractures of both materials revealed clear rate dependencies at room temperature. The fracture strengths of both materials increased with the stress rate over a range from about 10^{-1} MPa/s to 10^3 MPa/s and then remained almost constant from 10^3 MPa/s to 10^4 MPa/s. The rate dependency of the fracture strength in alumina ceramics was clearer than that of soda glass because the scatter of the fracture strengths in the alumina ceramics was smaller than that of soda glass. Stereomicroscope images of the fracture surface of soda glass and alumina ceramics are shown in Fig. 4. It is obviously seen that mirror, mist and hackle in the vicinity of the surface acting maximum stress. Therefore, the dynamic fatigue fractures of both materials are caused by SCG from an initial crack. The scatter of fracture strengths in both materials is directly related to the scatter of the initial crack sizes. The rate dependency in brittle materials such as those under discussion here agrees with findings in the literature [2, 3, 16].

Material constants of both models

Material constants of Model I

Figure 5 shows the least squares fit to plots of the fracture strength, σ_{\max} , and the effective loading time, t_{eff} , of soda

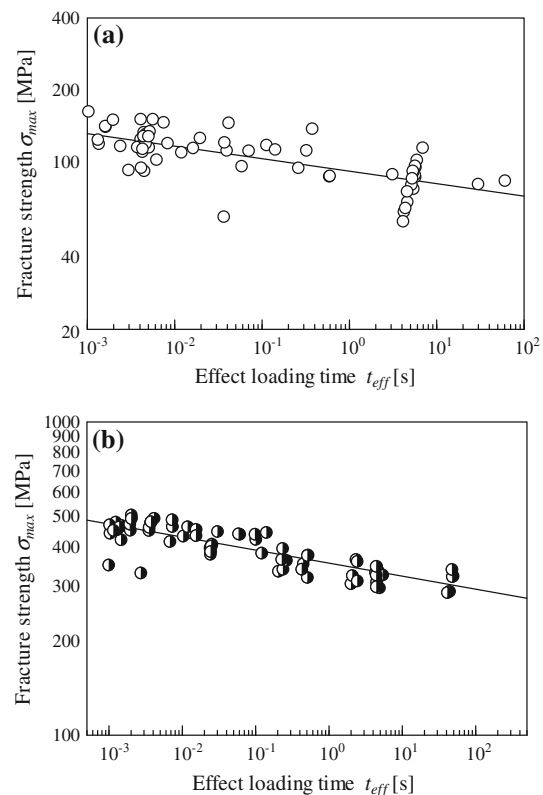


Fig. 5 σ_{\max} – t_{eff} plots and least squares fit of **a** soda glass and **b** alumina ceramics

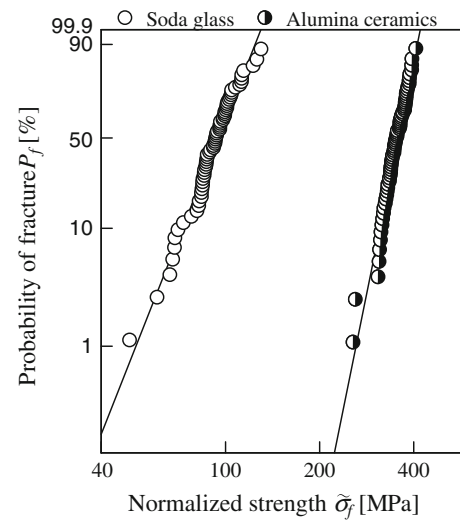


Fig. 6 Weibull plots of the normalized strengths of soda glass and alumina ceramics

glass and alumina ceramics. The crack propagation indices, n , of soda glass and alumina ceramics were 19.1 and 24, respectively. Figure 6 shows the Weibull plots of the normalized strengths of the soda glass and alumina ceramics. The Weibull plots of the normalized strengths of both materials obey a two-parameter Weibull distribution,

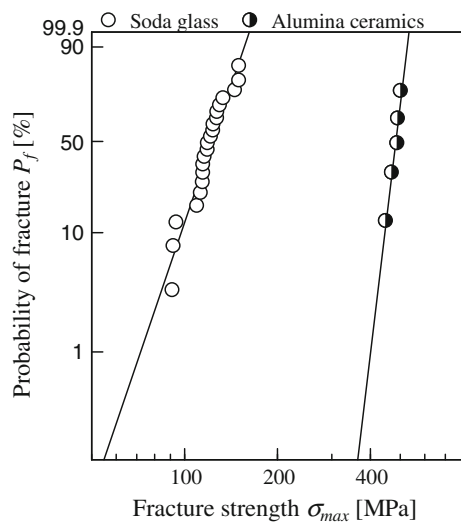


Fig. 7 Weibull plots of the fracture strengths of soda glass and alumina ceramics under a very fast stress rate

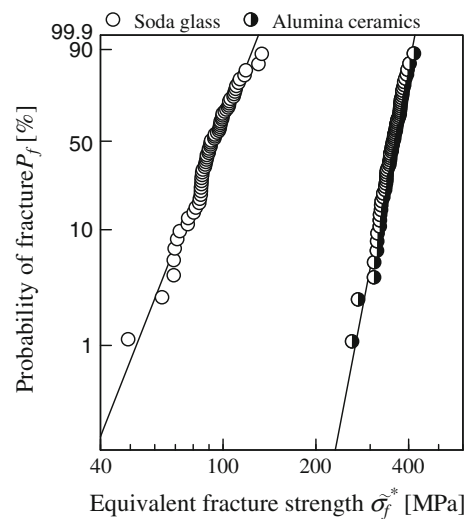


Fig. 9 Weibull plots of equivalent fracture strengths of soda glass and alumina ceramics

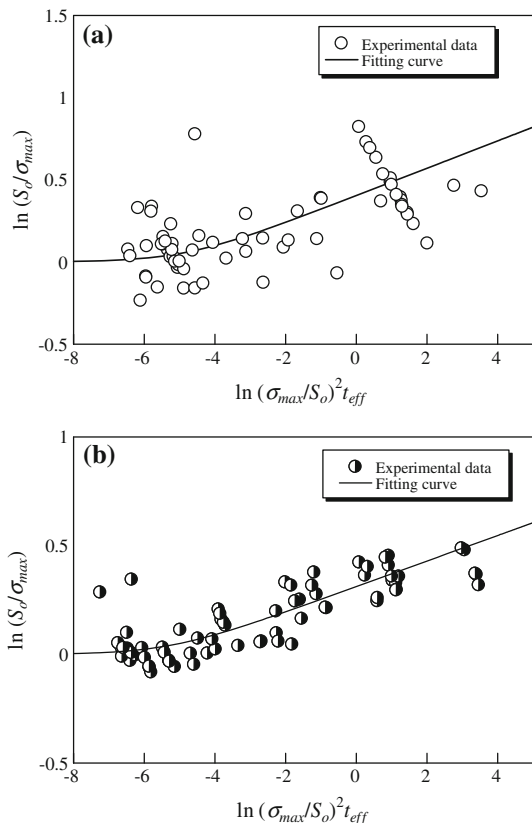


Fig. 8 Measured and fitted values of y versus x in Eq. 26 of **a** soda glass and **b** alumina ceramics

indicating that the dynamic fatigue fracture of brittle materials was not affected by a wide range of stress rates, only obeying the SCG concept. The shape and scale parameters of soda glass, \hat{m} and $\hat{\sigma}_o$, were 7.19 and 99.1 MPa, respectively.

Table 1 Material constants of soda glass and alumina ceramics

Materials	Soda glass	Alumina ceramics
Model I		
Crack propagation index, n	19.1	24
Shape parameter \hat{m}	7.19	14
Scale parameter $\hat{\sigma}_o$ (MPa)	99.1	365.4
Model II		
Shape parameter, m	8.15	23.1
Scale parameter, S_o (MPa)	127.9	490.8
Crack propagation index, n	14	19
Materials constant, t_o (s)	0.008	0.00531
Shape parameter \hat{m}	7.25	14.8
Scale parameter $\hat{\sigma}_o$ (MPa)	99.8	368

On the other hand, \hat{m} and $\hat{\sigma}_o$ of the alumina ceramics were 14 and 365.4 MPa, respectively.

Material constants of Model II

Figure 7 shows the Weibull plots of the fracture strength, σ_{max} , of soda glass under 100 mm/min and that of alumina ceramics under 200 mm/min. The shape and scale parameters of soda glass m and S_o were 8.15 and 127.9 MPa, respectively. On the other hand, m and S_o of the alumina ceramics were 23.1 and 490.8 MPa, respectively.

Figure 8 presents the experimental results for x and y in Eq. 26 of soda glass and alumina ceramics. By fitting these plots to $y = \{\ln(1 + x/t_o)\}/(n - 2)$ using the calculated S_o and the experimental data, we obtained $n = 14$ and $t_o = 0.008$ s for soda glass and $n = 19$ and $t_o = 0.00531$ s for alumina ceramics.

Figure 9 shows the Weibull plots of the equivalent fracture strengths of soda glass and alumina ceramics. The Weibull plots of the equivalent fracture strengths as well as those of the normalized strengths of both materials well obeyed a two-parameter Weibull distribution. The shape and scale parameters of soda glass \hat{m} and $\hat{\sigma}_o$ were 7.25 and 99.8 MPa, respectively. On the other hand, \hat{m} and $\hat{\sigma}_o$ of alumina ceramics were 14.8 and 368 MPa, respectively. Table 1 collectively lists the material constants of both materials from both Model I and Model II.

Dynamic effects on fatigue strength

The values of n (19.1 and 14) of soda glass calculated with both models nearly equaled those in the literature ($n = 13\text{--}25$ for soda glass [18]). On the other hand, the values of n (24 and 19) of alumina ceramics were lower than those in the literature ($n = 44\text{--}52$ for alumina ceramics [10]). These results indicated that though the dynamic effects on the degradation of the fatigue strength in soda glass can be ignored for a short period of failure, that of alumina ceramics cannot be ignored.

F–S–T diagrams described of both models and their comparison

The fracture times, t_f , are expressed by Eq. 10 in Model I and Eq. 19 in Model II, respectively, as follows:

$$t_f = (n+1) \left(\frac{\hat{\sigma}_o}{\sigma_{max}} \right)^n \sqrt[m/n]{-\ln(1-F)} \quad (27)$$

$$t_f = \frac{n+1}{\sigma_{max}^n} \left(\hat{\sigma}_o^n \sqrt[m/n]{-\ln(1-F)} - (n+1) S_o^2 \sigma_{max}^{n-2} t_o \right) \quad (28)$$

Figures 10 and 11 depict plots of the fracture strength, σ_{max} , and the fracture time, t_f , in soda glass and alumina ceramics and F–S–T diagrams predicted from Eqs. 27 and 28 using calculated material constants for both materials. Though the predictions from Eqs. 27 and 28 for both materials were in good agreement, the predictions from Eq. 28 in Model II were better in regards to the rate dependency in both materials explained in “**Dynamic fatigue behavior**” section. To verify the validity of the predictions of the two models, we calculated the correlation coefficients for the experimental plots and the predictions ($F = 63.2\%$) in both models for both materials using a CORREL function in Excel for Windows. Values of the correlation coefficients of soda glass were 0.719922 (Model I) and 0.714571 (Model II), respectively. On the other hand, values of correlation coefficients of alumina ceramics were 0.844399 (Model I) and 0.855916 (Model II), respectively. Values of the correlation coefficients of soda glass were almost equal because the scatter of the dynamic fatigue strength was large.

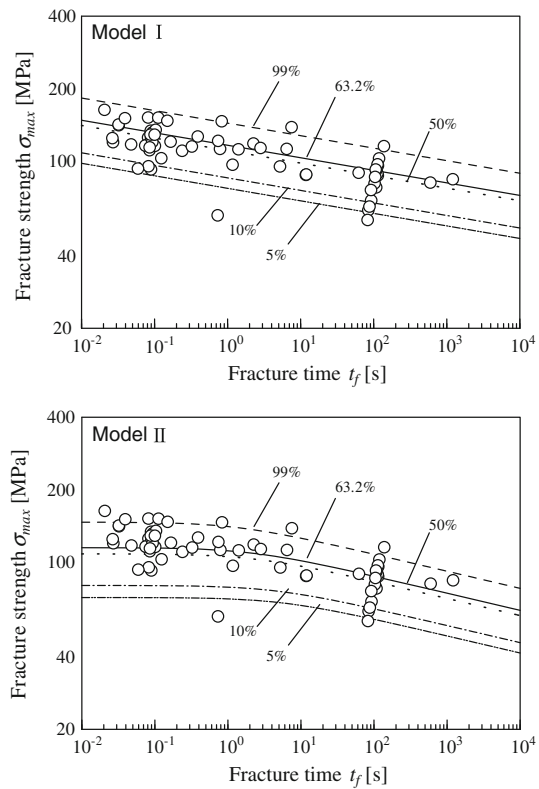


Fig. 10 σ_{max} – t_f plots and F–S–T diagrams predicted from Models I and II for soda glass

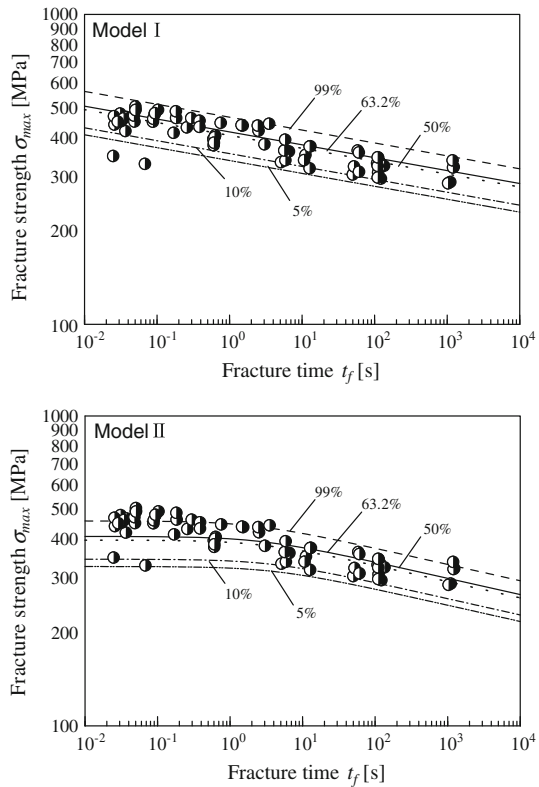


Fig. 11 σ_{max} – t_f plots and F–S–T diagrams predicted from Models I and II for alumina ceramics

In alumina ceramics, the value (0.855916) of the correlation coefficient from Eq. 28 was slightly larger than the value (0.844399) of that from Eq. 27. Therefore, the above results proved that Model II was more valid than Model I to estimate the relationship between the fracture strength, σ_{\max} , and the fracture time, t_f , in brittle materials in a quasi-static load test under a wide range of stress rates. We have considered that the predictions of Model II might even be in good agreement with the dynamic fatigue behavior under an even wider range of stress rates, and predicting brittle materials to having large scatter could be valid with an increased amount of data.

Conclusion

In this study, we estimated the dynamic fatigue strengths of soda glass and alumina ceramics under a wide range of stress rates using two probabilistic delayed-fracture models (Models I and II), which we derived from the SCG concept in conjunction with a two-parameter Weibull distribution. The predictions of Model II were better in regards to the stress rate dependency of the dynamic fatigue strengths for both materials than those of Model I. Particularly, the predictions of Model II for alumina ceramics resulted in better fitting to the experimental data compared to the predictions made for soda glass because the scatter of the dynamic fatigue strength of soda glass was large. These results proved that Model II was more valid than Model I to statistically estimate the dynamic fatigue strengths in brittle materials under a wide range of stress rates.

References

- Evans AG (1974) Int J Fract 10(2):251
- Evans AG, Johnson H (1975) J Mater Sci 10:214. doi:10.1007/BF00540345
- Futakawa M, Kikuchi K, Tanabe Y, Muto Y (1997) J Eur Ceram Soc 17:1573
- Barinov SM, Ivanov NV, Orlov SV, Shevchenko V (1998) Ceram Int 24:421
- Pan LS, Matsuzawa M, Horibe S (1998) Mater Sci Eng A 244: 199
- Evans AG (1980) Int J Fract 16(6):485
- Seshadri SG, Srinivasan M, Weber GE (1982) J Mater Sci 17:1297. doi:10.1007/BF00752238
- Guil F, Reece MJ, Vaughan DAJ (1991) J Mater Sci 26:3275. doi:10.1007/BF01124674
- Tanaka T, Nakayama H, Okabe N, Imamichi T (1995) Strength and crack growth behavior of sintered silicon nitride in cyclic fatigue. Cyclic fatigue in ceramics. Elsevier Science, Japan, p II345
- Ping Z, Zhongqin L, Guanlong C, Ikeda K (2004) Int J Fatigue 26:1109
- Davidge RW, McLaren JR, Tappin G (1973) J Mater Sci 8:1699. doi:10.1007/BF00552179
- Aoki S, Ohata I, Ohnabe H, Sakata M (1983) Int J Fract 21:285
- Kokubo T, Ito S, Shigematsu M, Sakka S (1987) J Mater Sci 22:4067. doi:10.1007/BF01133359
- Okabe N, Ikeda T (1991) Mater Sci Eng A 143:11
- Okabe N, Hirata H (1995) High temperature fatigue properties for some types of SiC and Si_3N_4 . Cyclic fatigue in ceramics. Elsevier Science, Japan, p 245
- Pfingsten T, Glien K (2006) J Eur Ceram Soc 26:3061
- Evans AG, Fuller ER (1974) Metall Trans 5:27
- Tokunaga H, Deng G, Ikeda K, Kaizu K (2005) Japan Soc Mech Eng A 71(712):1708